Electronic Supplementary Information

On the manuscript entitled:

Phosphocholine-decorated Superparamagnetic Iron Oxide Nanoparticles: defining the structure and probing *in vivo* application.

SPIONs synthesis.

SPIONs were synthesized through thermal decomposition method.[1] In detail 0.355 g of iron(III) acetylacetonate ($Fe(acac)_3$, 99%), 1.29 g of 1,2-hexadecanediol ($C_{14}H_{29}CH(OH)CH_2(OH)$, 90%), 1 ml of oleylamine (OAM, $C_9H_{18}=C_9H_{17}NH_2$, 70%), 1 ml of oleic acid (OA, $C_9H_{18}=C_8H_{15}$-COOH, 99%) and 10 ml of diphenyl ether ($C_{12}H_{10}O$, 99%), all purchased from Sigma Aldrich, were mixed together in a three neck flask. The solution was heated at 200 °C under argon atmosphere and vigorous stirring. After 2 h at reflux, the flask was removed from the heater and cooled to room temperature. The 1,2-hexadecanediol is chosen as reducing agent to convert the iron(III) salts in Fe_3O_4 oxide, which contains both Fe(II) and Fe (III), while oleic acid and oleylamine are introduced as stabilizing agents to prevent nanoparticle aggregation.

At the end of the synthesis, in order to allow the removal of undesired components, the suspension was treated with ~ 10 ml of ethanol and, after centrifugation at 7000 rpm for 20 min, the nanoparticles were obtained as a solid precipitate and then dispersed with cyclohexane.

Small Angle X-ray Scattering (SAXS)

Small Angle X-ray Scattering measurements at room temperature were performed at the beam line I22 of Diamond Light Source. The instrumentation associated with this beam line ensures high flux and brilliance, as well as high resolution and minimum beam divergence. The beam line operated at energy corresponding to 12.8 keV and a wavelength of 1 Å, while the detector was positioned at a distance of 6 m from the sample. This configuration allowed collecting data in the q range corresponding to 0.007-0.240 $Å^{-1}$, which resulted to be appropriate in order to have information on nanoparticle structure. The raw data were then corrected for the background. Detector efficiency correction, radial average and transformation to absolute scattering cross sections $d\Sigma/d\Omega$ were made using collagen as standard.

Also in this case the absolute scattering cross sections $d\Sigma/d\Omega$ dependence from the scattering vector q can be summarized with equation 4.

Characterization of SPIONs suspension in cyclohexane.

The synthesized SPIONs were coated by the layer composed by oleic acid and oleylamine molecules, which makes them stable in apolar solvents, such as cyclohexane. The chemical composition of the SPIONs was characterized by means of Wide Angle X-ray Scattering (WAXS) measurements. In particular, the SPIONs were deposited on an appropriate support by drop casting the cyclohexane suspension. From the collected WAXS data, reported in Figure S1(panel a), it is evident the typical peack pattern of the Fe_3O_4iron oxide, confirming the obtainment of the iron oxide with the appropriate stoichiometry responsible for the magnetic properties exhibited by SPIONs. Indeed, the typical S-shaped hysteresis loop of superparamagnetic nanoparticles was recorded for the synthesized SPIONs (Figure S1, panel b).

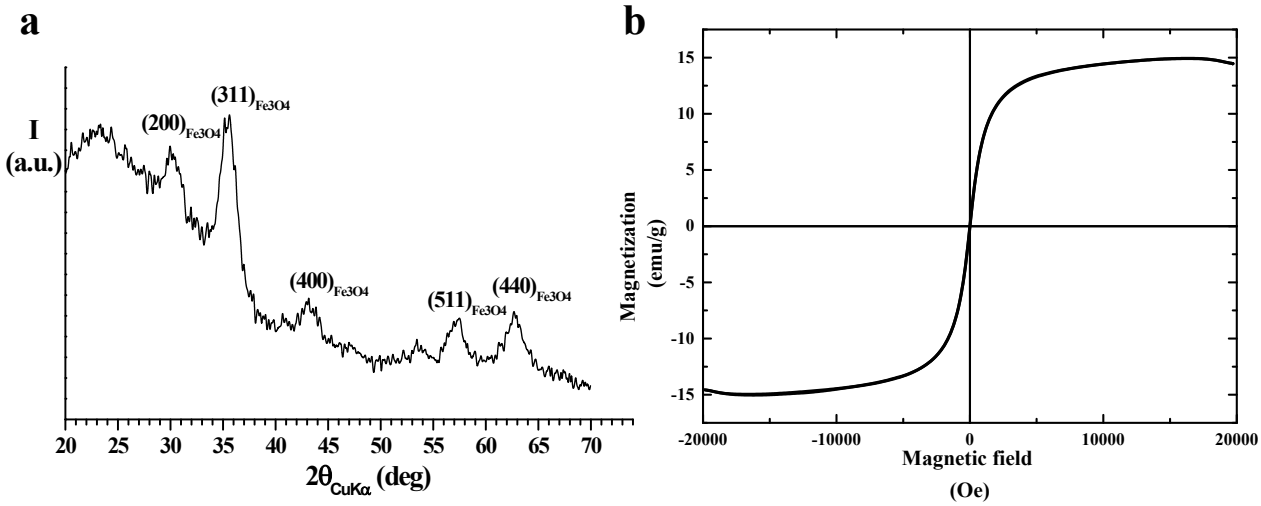

Figure S1: WAXS spectrum of dried SPIONs confirming the synthesis of Fe_3O_4 iron oxide nanoparticles (panel a) and hysteresis loop with the typical S-shape of superparamagnetic nanoparticles (panel b).

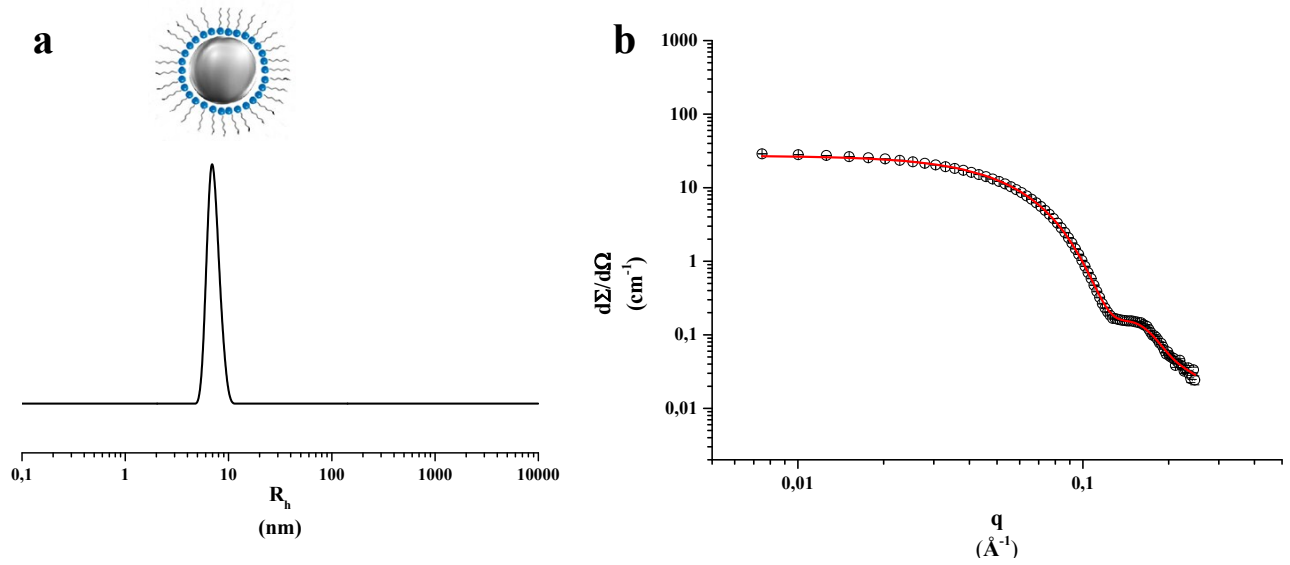

Figure S2: Hydrodynamic Radius Distribution (panel a) and SAXS data (panel b) for MNPs suspension in cyclohexane.

The hydrodynamic radius of the SPIONs in the cyclohexane suspension was evaluated by means of Dynamic Light Scattering (DLS) measurements. As shown in figure S2 (panel a) and table S1, a single population of nanoparticles with mean hydrodynamic radius corresponding to about 6 nm was observed. The estimated hydrodynamic radius takes into account of both the oleic acid and oleylamine shell, coating the iron oxide core, and of the solvation shells, which are diffusing with the SPIONs. Thus, the adopted synthetic protocol led to the obtainment of monodispersed nanoparticles.

In order to complete the information derived from the DLS measurements, and to further characterize the SPIONs size and shape, also Small Angle X-rays Scattering (SAXS) data and Transmission Electron Microscopy (TEM) images were collected.

SPIONs	
R_h (nm)	**r (nm)**
(6 ± 1)	(3.3 ± 0.4)

Table S1: Structural parameters obtained from DLS and SAXS data analysis for SPIONs suspension in cyclohexane.

Taking in consideration the X-ray scattering length densities of the different components that were present within the sample ($\rho^{X-ray}_{Fe_3O_4} = 4.1 \cdot 10^{-5}$Å^{-2}, $\rho^{X-ray}_{oleic\ acid} = 8.5 \cdot 10^{-6}$Å^{-2}, $\rho^{X-ray}_{oleylamine} = 7.8 \cdot 10^{-6}$Å^{-2} and $\rho^{X-ray}_{cyclohexane} = 7.5 \cdot 10^{-6}$Å^{-2}), it is evident that the X-rays represent a suitable tool to probe the SPIONs inorganic core. However, the information concerning the organic coating are lost due to the

small contrast in terms of scattering length density with respect to the solvent. The experimental data were treated as arising from a non-interacting suspension of sphere having scattering length density of the Fe_3O_4 iron oxide, according to the following equation:

$$P(q)=\frac{1}{V^2}\left[3V_C\left(\rho_{Fe_3O_4}-\rho_{cyclohexane}\right)\frac{\left(sin\left(qr\right)-qr\,cos\left(qr\right)\right)}{(qr)^3}\right]^2 \quad (5)$$

As showed in the figure S2 (panel b), a perfect agreement between the fitting curve and the experimental data was achieved, validating the adopted model. The extracted structural parameters are summarized in table S1.

The model used for SAXS data analysis was based on the assumption that the nanoparticles were spherical. Further confirmation of the results obtained through the scattering techniques measurements, TEM images were also recorded. In particular, a proper amount of the SPIONs cyclohexane suspension was dried onto a copper grid.

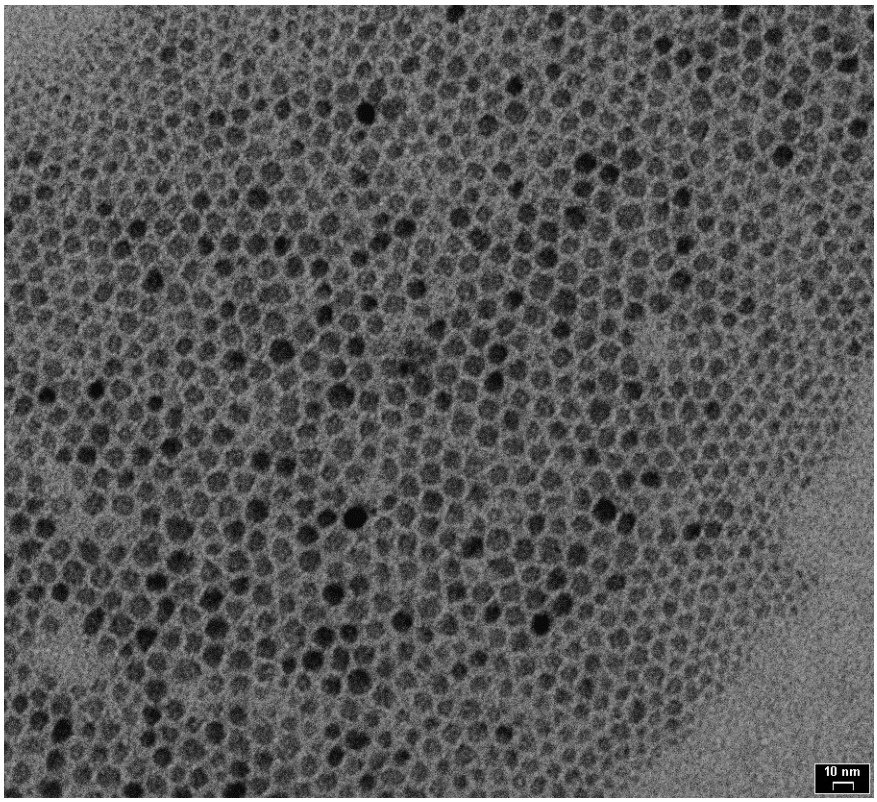

FigureS3: TEM image of SPIONs cyclohexane suspension dried on a copper grid.

Inspection of the image in the figure S3, confirm that the SPIONs can be indeed assimilated to a sphere whose size is comparable to values estimated with the other experimental techniques.

Characterization of ToThyCholRu-18LPC/SPIONs.

As it is shown from the hydrodynamic radius distribution reported in the main text (figure 2), two populations were present within the sample. Considering the average dimensions of the two populations it is reasonable to assume that the presence of ToThyCholRu has promoted the formation of small nanoparticle clusters with sizes less than 100 nm. However, those represent only a few % of nanoparticles present in the system. In fact since the scattered intensity depends on both the mass squared and the concentration of the scattering objects, the intensity distribution can be converted in a concentration distribution normalizing the scattering intensity in the approximation that $M \sim R_h$ where M is the mass and R_h is the hydrodynamic radius. In the present case we are dealing with spherical objects so that $M : kR_h^3$. Thus, the relative amount of the two populations observed in the 18LPC-ToThyCholRu/SPIONs was estimated (figure S4 panel a, red curve). It is worth noting that the assumption of spherical objects though with a larger size was subsequently verified also in the case of the nanoparticle clusters by means of SANS measurements and Cryo-TEM images. From figure S4 (panel a) as mentioned it is evident that the nanoparticle clusters are indeed a small fraction if compared with the population of single functionalized nanoparticles.

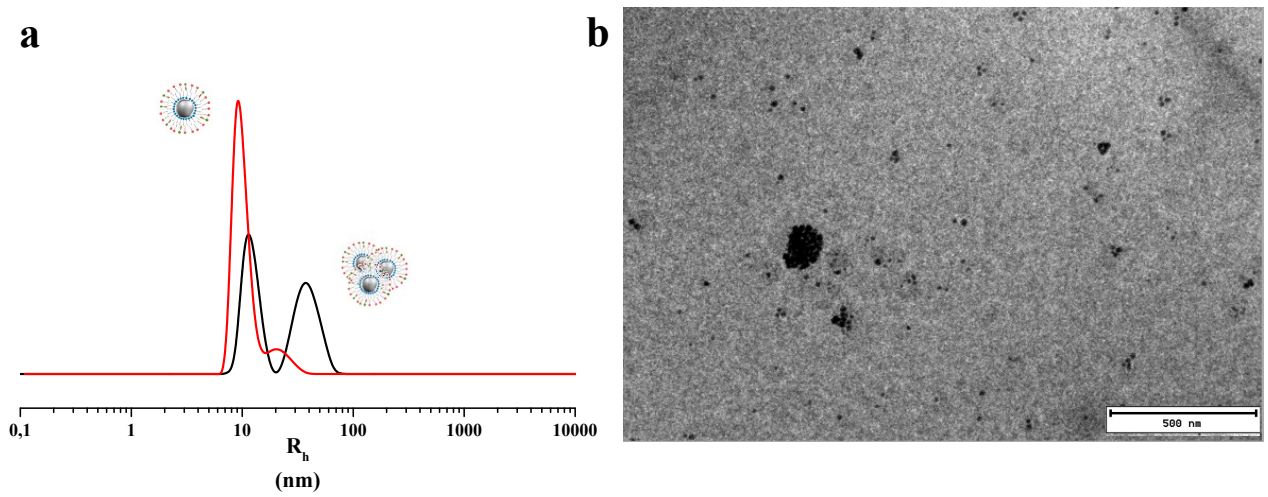

Figure S4: Hydrodynamic radius intensity distribution(black curve) together with the result of mass distribution conversion (red curve). Cryo-TEM image identifying the spherical shape of the nanoparticle cluster is showed in panel b.

A further validation of the results obtained through the light and neutron scattering experiments was achieved by recording Cryo-Trasmission Electron Microscopy (Cryo-TEM) images on the 18LPC-ToThyCholRu/SPIONs suspension. In particular, as showed in figure S4 (panel b), the nanoparticles

clusters present in the 18LPC-ToThyCholRu/SPIONs can be reasonably considered spherical. Indeed, the observation of clusters with an almost spherical shape, represented by an agglomerate of single SPIONs, was used in the interpretation of the collected SANS data.

As discussed in the main text, in principle the appropriate equation that should be used to analyse the neutron scattering data, should include two form factors, accounting for single functionalized SPIONs and clusters, as well as a structure factor arising from hard sphere interaction between the SPIONs composing the cluster. Each of this term has to be multiplied by the corresponding volume fraction. Considering that the percentage of clusters with respect to the total number of particles present in the suspension is very low (about 10%), we decided to simplify the model for the fitting of the SANS data by neglecting the structure factor and considering only the sum of the two form factors weighted by the corresponding volume fractions. The advantage of this simplification is that a smaller number of parameters has to be optimized during the fitting procedure.

In the figure S5 each of the contributions to the total scattered intensity were separately plotted together with the experimental data. In particular, the two form factors as separate curves and as summed curve are reported according to the legend. Furthermore, the structure factor calculated according to the SPIONs size and considering a high packing degree of the nanoparticles within the cluster (0.7 volume fraction), as suggested by the Cryo-TEM image, is as well reported. As it is possible to observe, the structure factor predicts a correlation peak at q= 0.018 $Å^{-1}$, which clearly corresponds to a region where the cluster and the single SPION form factors have a stronger contribution to the scattered intensity. Moreover, it has to be considered that, in order to make clearer its features, the structure factor reported in the graph was not multiplied by the volume fraction of the cluster within the suspension. However, if the cluster volume fraction is taken into account scattering intensity will became very low. Furthermore if the nanoparticles in the cluster are somewhat disordered and/or even their volume fraction is lower, than above imposed, the peaks in S(q) drastically reduce. According to all these consideration, we concluded that the SANS data pattern was mostly governed by the cluster and single SPION form factors.

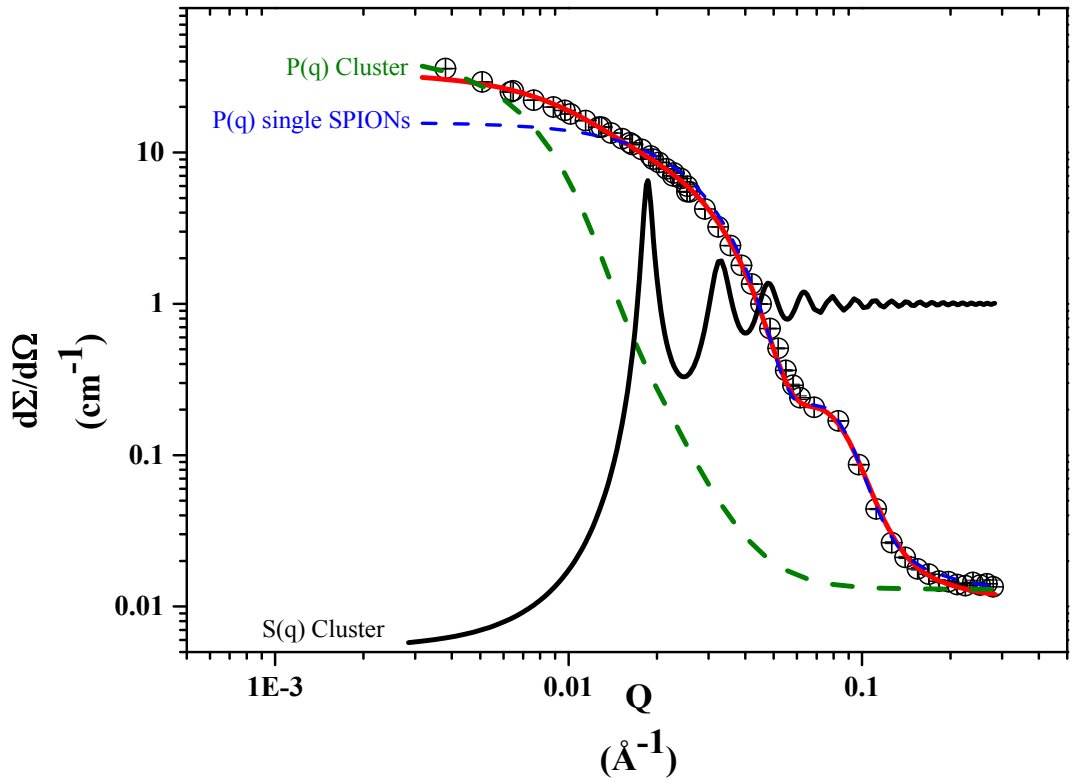

Figure S5: SANS data collected for the 18LPC-ToThyCholRu/SPIONs together with the fitting curve (red) obtained by summing the cluster and the single SPIONs form factors. The cluster and single SPIONs form factor are also reported as separate curves (respectively dashed green and blu curves). The simulated structure factor for the SPIONs constituting the cluster is as well reported (black curve).

A possible interpretation of nanoparticle cluster formation in the case of 18LPC-ToThyCholRu/SPIONs is based on the structure of ToThyCholRu. Indeed, ToThyCholRu is too large and rigid, if compared to 18LPC, to respect the curvature radius imposed by the inorganic iron oxide core. On the other hand, the smaller curvature radius associated with the cluster surface might represent a more stable situation for the ToThyCholRu to be lodge within the 18LPC layer.

Cell Cultures.

Human HaCaT keratinocytes , murine 3T3L-1 fibroblasts, human Calu-6 and A549 lung carcinoma cell lines were grown in Dulbecco's modified Eagle's medium (DMEM, Invitrogen, Paisley, UK) containing high glucose (4.5 g/l), while human MCF-7 breast adenocarcinoma cells were grown in RPMI 1640 medium (Invitrogen, Paisley, UK). Media were supplemented with 10% fetal bovine

serum (FBS, Cambrex, Verviers, Belgium), L-glutamine (2 mM, Sigma, Milan, Italy), penicillin (100 units/ml, Sigma) and streptomycin (100 mg/ml, Sigma). All the cells were cultured in a humidified 5% carbon dioxide atmosphere at 37 °C.

The nanoparticles bioactivity was investigated by the estimation of a "cell survival index", arising from the combination of cell viability evaluation with cell counting. The cell lines were washed with PBS buffer solution (Sigma), collected by trypsine (Sigma) and then inoculated in a 96-microwell culture plates at density of 10^4 cells/well. Cells were allowed to grow for 48 h, then the medium was replaced with fresh medium and treated for further 48 h with different total lipid concentrations of the ruthenium-free 18LPC/SPIONs (60, 100 and 200 μM, corresponding to 30, 50 and 100 μg/ml of iron concentration, respectively) and of the ruthenium-containing 18LPC-ThyCholRu/SPIONs (10% in moles with respect to the total lipid concentration). Using the same experimental procedure, cell cultures were also incubated with the low molecular weight ruthenium complex AziRu and cisplatin (*c*DDP), as positive control for cytotoxic effects. Cell viability was evaluated with MTT assay, which measures the level of mitochondrial dehydrogenase activity using the yellow 3-(4,5-dimethyl-2-thiazolyl)-2,5-diphenyl-2H tetrazolium bromide (MTT, Sigma) as substrate. The assay was based on the redox ability of living mitochondria to convert dissolved MTT into insoluble purple formazan. Briefly, after the treatments the medium was removed and the cells were incubated with 20 μl/well MTT solution (5 mg/ml) for 1 h in a humidified 5% CO2 incubator at 37 °C. The incubation was stopped by removing the MTT solution and by adding 100 μl/well of DMSO to solubilize the purple formazan. Finally, the absorbance was monitored at 550 nm by using a microplate reader (iMark microplate reader, Bio-Rad, Milan, Italy).

Cell number was determined by TC20 automated cell counter (Bio-Rad, Milan, Italy), providing an accurate and reproducible total count of cells and a live/dead ratio in one step by a specific dye (trypan blue) exclusion assay. Following the same principle used in hemocytometers, Bio-Rad's TC20 automated cell counter uses disposable slides, TC20 trypan blue dye (filter-sterilized 0.4% trypan blue dye w/v in 0.81% sodium chloride and 0.06% potassium phosphate dibasic solution) and a CCD camera to count cells based on the analyses of captured images. Once the loaded slide is inserted into the slide port, the TC20 automatically focuses on the cells, detects the presence of trypan blue dye and provides the count. When cells are damaged or dead**,** *trypan blue* can enter the cell allowing dead cells to be counted. Operationally, after bioscreen incubations in standard 96-microwell culture plates, the medium was removed and the cells were collected. Ten microliters of cell suspension, mixed first with 0.4% trypan blue solution at 1:1 ratio, were directly loaded into the chambers of disposable slides. The results are displayed as total cell count (number of cells/ml). If trypan blue is detected, the instrument also accounts for the dilution and shows live cell count and percent viability. Total counts

and live/dead ratio fromrandom samples for each cell line were subjected to comparisons with manual hemocytometers in control experiments.

The calculation of the concentration required to inhibit the net increase in the cell number and viability by 50% (IC_{50}) was based on plots of data carried out in triplicates and repeated five times (total n =15). IC_{50} values were obtained using a dose-response curve by nonlinear regression using a curve fitting program, GraphPadPrism 5.0, and are expressed as mean ± SEM (n = 15).

Statistical Analysis

All data were presented as mean ± SEM. The statistical analysis was performed using Graph-Pad Prism (Graph-Pad software Inc., San Diego, CA) and ANOVA test for multiple comparisons was performed followed by Bonferroni's test.

MRI Measurements

Phantom studies

A phantom was prepared consisting of a culture cell plate containing MNPs in H_2O and 1% agar gel solutions at different concentrations (from 0.016 mM up to 2.5 mM, [Fe] concentration) located in the plate wells. The T_1 and T_2 relaxation profiles of the NPs were then assessed at 1.5 and 3 T using clinical scanners (1.5 T Signa Excite and 3 T Signa HDxT, GE Healthcare, USA, respectively). The reception of the MR signal was performed using a clinical head coil to increase the filling factor with the phantom placed at the center of the coil.

The longitudinal (T_1) relaxation time of the solutions was measured using a standard Inversion Recovery (IR) with the following parameters: TR = 9000, TE = 7.6 ms at 3 T and 6.7 at 1.5 T, TI = 100 – 2100 ms in steps of 200 ms, FOV = 18x18 cm for 3 T and 23x23 cm at 1.5 T, matrix 192x192 pixels, slice thickness = 3 mm.

The transverse (T_2) relaxation time was measured with a T_2-weighted Spin Echo sequence using the following parameters: TR = 1500 ms at 3 T and 1000 ms at 1.5 T; TE = 5.2 – 160.3 ms at 1.5 T and 6.9 – 110.1 ms at 3 T; 16 scans, FOV = 16x16 cm at 3 T and 23x23 cm at 1.5 T, matrix 192x192 pixels, slice thickness = 7 mm.

To evaluate the effect of low field on T_2-relaxivity we used an 0.32 T open magnet and 0.5 T open magnet (MrOpen, Paramed Medical System), with a dedicated head multi-array coils: a 2-dimensional acquisitions were obtained: proton density (PD)–weighted oblique coronal and oblique sagittal planes, T2-weighted fast spin echo (FSE) oblique coronal and oblique axial planes, gradient echo (GRE) oblique axial plane, and short tau inversion recovery (STIR) oblique coronal plane.

The longitudinal (R_1) and transverse (R_2) relaxation rates were calculated as the inverse of T_1 and T_2 relaxation times, respectively. The longitudinal (r_1) and transverse (r_2) relaxivity (expressed in mM^{-1} s^{-1} [Fe] concentration) were then estimated as the slope of the regression line obtained for R_1 and R_2 versus the NPs concentration.

18LPC/SPIONs and 18LPC-ToThyCholRu/SPIONs in vitro bioscreens.

The obtained results are reported both in terms of concentration–effect bar graphs (Figure S6) and of IC_{50} values (Table S2).

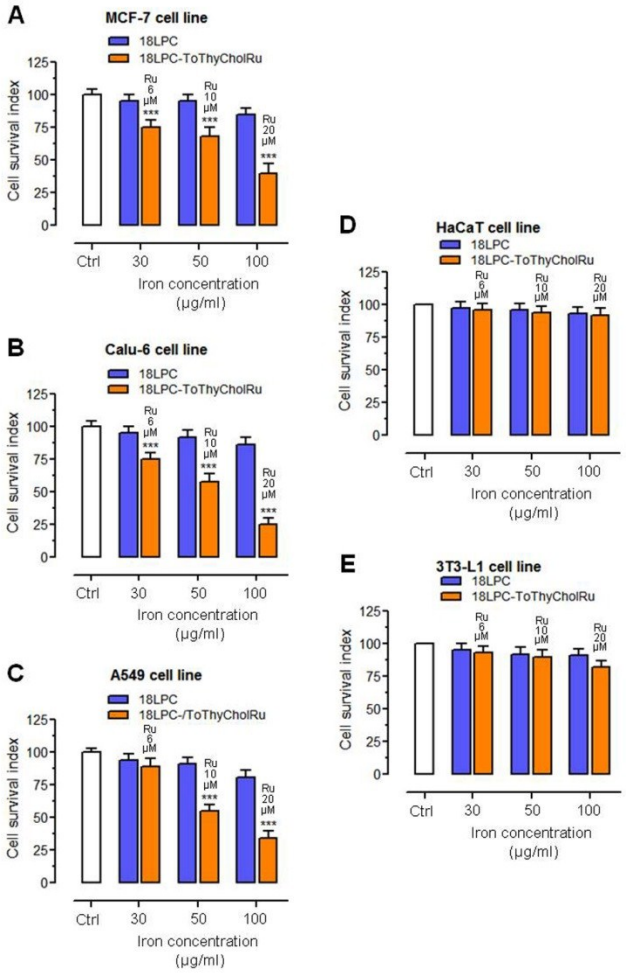

Figure S6: *Cell survival index, evaluated by the MTT assay and the live/dead cell ratio, for human breast adenocarcinoma MCF-7 cells (panel A), lung carcinoma Calu-6 (panel B) and A549 cells (panel C), and for human HaCaT keratinocytes (panel D) and murine 3T3-L1 fibroblasts (panel E) following 48 h of incubation with the indicated iron concentration (µg/ml) of 18LPC/SPIONs and of the ruthenium-containing 18LPC-ToThyCholRu/SPIONs, as indicated in the legend. In graphs, on bar tops the actual ruthenium amounts within functionalized 18LPC-ToThyCholRu/SPIONs are indicated. Data are expressed as percentage of untreated control cells and are reported as mean of five independent experiments.*

In the IC_{50} table (table S2), data concerning cisplatin (*c*DDP) are included for comparison, as a positive control for cytotoxic effects.

Table of the IC_{50} values

Cell lines	***cDDP***	***18LPC-ToThyCholRu/ SPIONs***
MCF-7	22 ± 4 μM	**17 ± 5 μM**
Calu-6	45 ± 5 μM	**12 ± 4 μM**
A549	36 ± 4 μM	**14 ± 5 μM**
HaCaT	272 ± 7 μM	**>100 μM**
3T3-L1	205 ± 6 μM	**>100 μM**

Table S2: *Comparison of the IC_{50} values (μM) relative to cisplatin (cDDP) and to the effective ruthenium concentration carried by 18LPC-ToThyCholRu/SPIONs in the indicated cell lines following 48 h of incubation.*

As previously described, 18LPC-ToThyCholRu/SPIONs enclose, in the external layer, only the 10% in moles of the active ruthenium complex with respect to their total lipid concentration: this must be taken into account in interpreting the ruthenium complex-dependent antiproliferative patterns shown in Figure 3, as well as in the results normalization according to the actual ruthenium complex amounts contained within 18LPC-ToThycholRu/SPIONs (6, 10 and 20 μM, respectively). In terms of ToThyCholRu concentration, IC_{50} values for 18LPC-ToThyCholRu/SPIONs are in the 10 to 20 μM range for human cancer cells, *i.e.* reflect those we have recently reported for ruthenium-based nanosystems with high antiproliferative activity *in vitro*.[2-6] To further highlight the biocompatibility features of 18LPC/SPIONs and

MRI (Phantom studies)

The 18LPC/SPIONs and the corresponding systems including the ruthenium complex ToThyCholRu have been initially tested in phantom systems at 1.5 and 3 T to evaluate their efficacy as negative MRI contrast agents at clinical magnetic fields. The phantoms consisted of culture cell plates containing the functionalized SPIONs in H_2O and 1% agar gel solutions at different concentrations. These experiments were fundamental to assess the capacity of 18LPC/SPIONs to simultaneously increase transverse (r_2, mM^{-1} s^{-1}) and decrease longitudinal (r_1, mM^{-1} s^{-1}) Magnetic Resonance (MR) relaxivities of water proton, leading to a notably high r_2/r_1 ratio and thus proving the functionalized-SPIONs to be sensitive MRI contrast agents.[7, 8] Both the longitudinal and the transverse proton relaxation rates, respectively indicated as R_1 and R_2, and corresponding to the inverse of the longitudinal and transverse relaxation time ($R_{1,2} = 1/T_{1,2}$ s^{-1}), increased in a linear trend upon

increasing the 18LPC/SPIONs concentration in the magnetic field range studied. This effect was quantified through the longitudinal and transverse relaxivities r_1 and r_2, representing the proton relaxation rates per SPIONs concentration unit (mM). As expected, the iron oxide core of the SPIONs induced a major effect on the transverse (T_2) rather than longitudinal (T_1) relaxation time (table S3). The 18LPC/SPIONs showed higher r_2 values for 1% agar compared to H_2O solutions (both at 1.5 and 3 T), demonstrating an increased contrast enhancement when dissolved in agar gel rather than H_2O. We speculate that this effect was due to the increased viscosity and decreased water diffusion coefficient compared to H_2O solutions.[9] According to the tissue-like nature of the agar gel phantoms used, this suggests the high potential of the tested system for the biological exploitation. The r_2/r_1 ratios were then calculated for 1% agar gel solutions, which showed significantly higher values compared to other available commercial systems[10], suggesting the efficacy of the tested SPIONs as a negative contrast agents for MRI.[11] Moreover, the same trend for the r_2 relaxivity was maintained even at the lower magnetic field strengths in the range 0.5 – 3 T. In particular, a substantially higher value of r_2 was already observed at 0.3 T, suggesting a possible increased contrast ability at the lowest field strength (r_2 = 38.4 s^{-1} mM^{-1} at 0.5 T and 61.1s^{-1} mM^{-1} and at 0.3 T, respectively, for agar gel solutions).

Table of relaxivities

	1.5 T		***3 T***	
	H_2O	***Agar gel1%***	***H_2O***	***Agar gel 1%***
r_2 (mM^{-1} s^{-1})	16.6	39.7	14.6	38.4
r_1 (mM^{-1} s^{-1})	-	$7.8 \cdot 10^{-1}$	$2.2 \cdot 10^{-1}$	$3.3 \cdot 10^{-1}$
r_2/r_1	-	51	66	122

Table S3: *Values of r_1 and r_2 relaxivity and r_2/r_1 ratios obtained at 1.5 and 3 T for the 18LPC/SPIONs in H_2O and 1% agar gel solutions.*

The presence of the amphiphilic ruthenium complex in the 18LPC-ToThyCholRu /SPIONs did not significantly alter the contrast enhancement with respect to the 18LPC/SPIONs, thus demonstrating that advanced imaging properties are preserved. In this case the ligand-size of the amphiphilic ruthenium complex did not induce significant variation of the longitudinal (r_1) and transverse (r_2) water proton relaxivities of 18LPC/SPIONs: this information is of relevant importance because the

MR image quality depends on r_1 and r_2 values, and in this case r_2 should be large for T_2 MRI contrast agents.

References:

1. S. Sun, H. Zeng, D. B. Robinson, S. Raoux, P. M. Rice, S. X. Wang and G. Li, *J Am Chem Soc*, 2004, **126**, 273-279.
2. G. Mangiapia, G. Vitiello, C. Irace, R. Santamaria, A. Colonna, R. Angelico, A. Radulescu, G. D'Errico, D. Montesarchio and L. Paduano, *Biomacromolecules*, 2013, **14**, 2549-2560.
3. D. Montesarchio, G. Mangiapia, G. Vitiello, D. Musumeci, C. Irace, R. Santamaria, G. D'Errico and L. Paduano, *Dalton Trans*, 2013, **42**, 16697-16708.
4. L. Simeone, G. Mangiapia, G. Vitiello, C. Irace, A. Colonna, O. Ortona, D. Montesarchio and L. Paduano, *Bioconjugate chemistry*, 2012, **23**, 758-770.
5. G. Vitiello, A. Luchini, G. D'Errico, R. Santamaria, A. Capuozzo, C. Irace, D. Montesarchio and L. Paduano, *J Mater Chem B*, 2015, **3**, 3011-3023.
6. G. Mangiapia, G. D'Errico, L. Simeone, C. Irace, A. Radulescu, A. Di Pascale, A. Colonna, D. Montesarchio and L. Paduano, *Biomaterials*, 2012, **33**, 3770-3782.
7. H. B. Na, I. C. Song and T. Hyeon, *Advanced Materials*, 2009, **21**, 2133-2148.
8. L. Menichetti, L. Manzoni, L. Paduano, A. Flori, C. Kusmic, D. De Marchi, S. Casciaro, F. Conversano, M. Lombardi, V. Positano and D. Arosio, *Ieee Sens J*, 2013, **13**, 2341-2347.
9. J. W. M. Bulte, J. Vymazal, R. A. Brooks, C. Pierpaoli and J. A. Frank, *Journal of Magnetic Resonance Imaging*, 1993, **3**, 641-648.
10. A. Ruiz, G. Salas, M. Calero, Y. Hernández, A. Villanueva, F. Herranz, S. Veintemillas-Verdaguer, E. Martínez, D. F. Barber and M. P. Morales, *Acta Biomaterialia*, 2013, **9**, 6421-6430.
11. W. J. M. Mulder, G. J. Strijkers, G. A. F. van Tilborg, A. W. Griffioen and K. Nicolay, *Nmr Biomed*, 2006, **19**, 142-164.